(11) Lovinger, A. J.; Davis, D. D.; Padden, F. J., Jr. *Polymer* **1985**, *26*, 1595.
(12) Cheng, S. Z. D.; Chen, J.; Janimak, J. J. *Polymer*, to be submitted for publication.
(13) Lazcano, S.; Fatou, J. G.; Marco, C.; Bello, A. *Polymer* **1988**, *29*, 2076.
(14) Hoffman, J. D.; Davis, G. T.; Lauritzen, J. I., Jr. In *Treatise on Solid-State Chemistry*; Hannay, N. B., Ed.; Plenum Press: New York, 1976; Vol. 3, Chapter 7.
(15) Vasanthakumari, R.; Pennings, A. J. *Polymer* **1983**, *24*, 175.
(16) Alamo, R.; Fatou, J. G.; Guzman, J. *Polymer* **1982**, *23*, 379.
(17) Organ, S. J.; Keller, A. *J. Polym. Sci., Polym. Phys. Ed.* **1986**, *24*, 2319.
(18) Pelzbauer, Z.; Galeski, A. *J. Polym. Sci., Part C* **1972**, *38*, 23.
(19) Roitman, D. B.; Marand, H. L.; Hoffman, J. D. *Bull. Am. Phys. Soc.* **1988**, *33*, 248.
(20) Barham, P. J.; Keller, A.; Otun, E. L.; Holmes, P. A. *J. Mater. Sci.* **1984**, *19*, 2781.
(21) Clark, E. J.; Hoffman, J. D. *Macromolecules* **1984**, *17*, 878.
(22) Sadler, D. M. *Polymer* **1983**, *24*, 1401.
(23) Sadler, D. M. *Polymer* **1987**, *28*, 1440.
(24) Allen, R. C.; Mandlekern, L. *Polym. Bull.* **1987**, *17*, 473.
(25) Padden, F. J., Jr.; Keith, H. D. *J. Appl. Phys.* **1959**, *30*, 1479.
(26) Norton, D. R.; Keller, A. *Polymer* **1985**, *26*, 704.
(27) Tanabe, Y.; Strobl, G. R.; Fischer, E. W. *Polymer* **1986**, *27*, 1147.
(28) Hoffman, J. D.; Weeks, J. J. *J. Res. Natl. Bur. Std., Sect. A* **1962**, *66A*, 13.
(29) Wunderlich, B. *Macromolecular Physics, Crystal Melting*; Academic: New York, 1980; Vol. 3.
(30) Fatou, J. G. *Eur. Polym. J.* **1971**, *7*, 1057.
(31) Hoffman, J. D.; Miller, R. L. *Macromolecules* **1988**, *21*, 3038.
(32) Bassett, D. C.; Olley, R. H. *Polymer* **1984**, *25*, 935.
(33) Lotz, B.; Wittmann, J. C. *J. Polym. Sci., Polym. Phys. Ed.* **1986**, *24*, 1541.

Flow-Induced Liquid–Liquid Phase Separation and Adsorption Entanglement Layer Formation in High Molecular Weight Polymer Solutions

P. J. Barham* and A. Keller

H. H. Wills Physics Laboratory, University of Bristol, Bristol BS8 1TL, U.K.
Received December 12, 1988; Revised Manuscript Received March 27, 1989

ABSTRACT: Rheological studies of very high molecular weight poly(methyl methacrylate) (PMMA) solutions have revealed three distinct types of anomalous behavior. These are interpreted, at low rates, as being due to the formation of topological adsorption–entanglement layers; at intermediate rates, to the nucleation by adsorption–entanglement layers of a flow-induced liquid–liquid phase separation; and at high rates, to a spontaneous liquid–liquid phase separation. An attempt has been made to construct the phase diagram for the binary system PMMA–dimethyl phthalate by using shear stress, as well as temperature and solution concentration, as thermodynamic variables.

Introduction

There have, over the past 30 or so years, been many reports of anomalous flow behavior in solutions of very high molecular weight polymers (e.g., ref 1–25). In particular in flow systems operating at constant stress (e.g., capillary flows) a decrease in flow rate with increasing flow time has been noted[13–18], and in systems operating at constant flow rate (e.g., Couette flow) the shear stress has been seen to rise during flow[1–10] and in some cases to fluctuate wildly.[10,23,26] It has been shown[18,26–30,32] that such behavior is associated with the formation of layers at surfaces of the viscometers. These layers, which are much thicker than the radius of gyration of polymer molecules, are called "adsorption–entanglement layers" and are believed to be formed by the mutual entanglement of molecules in the flowing solution and those adsorbed along the surfaces.

It has become apparent to us recently that the layers created by flow can be divided into two distinct classes according to their thickness. The first class, type I, as they will be referred to in the following, have a thickness of no more than several micrometers. Such layers are most usually formed in good solvents and at low flow rates. In capillary flow, for example, they cause a decrease in the flow rate, which, after some time, reaches a steady value. These layers can be difficult to detect and, in certain circumstances, can lead to significant error in the actual measurement of viscosity.[31] The second type of behavior (type II) is principally exhibited in poorer solvents at high rates; these layers grow thicker seemingly without limit and can fill the whole flow cell (thicknesses are thus comparable with the dimensions of the equipment and can easily reach several millimeters). Such behavior can result in completely blocked capillaries[27,32] and in Couette and cone and plate geometry leads to dramatic fluctuations in the observed shear and normal stresses.[1–11,26] In such cases some authors also report the observation of "gel-like" particles associated with this behavior (e.g., ref 11).

Recently, Rangel-Nafaile et al.[33] have observed rheological behavior of the same character as type II above, accompanied by the observation of turbidity in the flowing polystyrene solutions. They have consequently attributed their observations, together with many other previous reports on similar rheological observations,[1–23] to a flow induced liquid–liquid phase separation, as opposed to the formation and growth of an adsorption–entanglement layer. Rangel-Nafaile et al. argue that it is the shear stress on the solution that causes a shift in the phase boundaries and leads to liquid–liquid phase separation. The evidence for phase separation comes from observation of turbidity in the solution. Independently, Wolf has come to the same conclusion of liquid–liquid phase

0024-9297/90/2223-0303$02.50/0

separation through observation of similar effects.[34,35]

The purpose of the present work is to attempt to distinguish between flow-induced liquid–liquid phase separation—which is a pseudoequilibrium process—and the formation of "adsorption–entanglement" layers—which is a purely topological process of entanglement formation stabilized by flow. In order to distinguish these processes, it is necessary to devise suitable experiments. At first sight this may appear trivial: turbidity should demonstrate the presence of two phases and an identifiable layer along a foreign solid surface should indicate the presence of adsorbtion–entanglement layers. However, it can be readily argued (see below) that both phase segregation and adsorption–entanglement layers can lead to either of the two above-mentioned effects.

Consider those systems in which turbidity and/or gel particles have been observed:[10,11,33-35] these always show the type II behavior described above. However, such behavior in Couette flow has in the past been directly associated with the repeated building up and breaking down of a thick layer at the Couette wall.[26] If thick adsorption–entanglement layers are formed, and grow right across the flow cell, they will be eventually broken up by the flow itself, when the remnants of the layers would form transient gellike particles. If the latter are of a suitable size, they will scatter light and the flowing solution would appear turbid. Thus the observation of turbidity on its own need not necessarily be indicative of the presence of two equilibrium phases, as it cannot distinguish between all possible origins of the turbidity; i.e., in the present cases whether it is due to flow induced, liquid–liquid phase segregation or to the gellike particles of a topologically formed adsorption–entanglement layer.

Consider next systems where thick stationary layers can be seen to be built up during flow. At first sight this would appear to constitute unequivocal evidence for adsorption–entanglement layer formation. However, it is believed that the liquid–liquid phase segreation will occur where the shear stress is highest—that is, in most cases, at the walls of a flow cell. Thus a stationary layer may only represent a concentrated, separated phase that remains at the surface due to physical adsorption.

In conclusion, we see that neither the observation of turbidity nor that of distinct layers at the walls can conclusively decide in favor of either of the two alternatives, flow-induced liquid–liquid phase separation and flow-induced absorbtion–entanglement layers, each of which seems well supported in itself in the respective works, both by supplementary experimental material and by theory presented. In what follows the theoretical background for both alternatives will be recapitulated. For the adsorption–entanglement layer a model has been set up[30] according to which the first step is the formation of a layer of physically adsorbed molecules that have long loops that trail out into the solution. Occasionally, a passing molecule will have a suitable configuration (e.g., its end may be dangling outside the main coil) to become entangled with these loops. Such entanglements will be provided by flow, both by stabilizing them and by enhancing the rate of their formation. If we consider that flow constantly sweeps new molecules past a stationary layer, thus enhancing the number of molecules that come in contact, all in different configurations, it will be evident that this will not only stabilize entanglements already formed but will promote formation of new ones at a rate that by calculation[30] can easily account for the observations. This model suggests a simple experiment. If an oscillating (rather than continuous) flow is applied, then many fewer *different* molecules will pass by the surface so fewer configurations will be sampled, making entanglements less likely to occur. Further, when the direction of flow changes it is likely to reduce the stability of the entanglements and may even lead to actual disentanglement.

The effect of an oscillatory flow field on stress-induced liquid–liquid phase separation should be much less severe. If a constant shear rate is applied but the sense of rotation periodically reversed, then the resulting shear stress will have a constant magnitude and the first normal stress difference will remain constant (except at the times when the sense of rotation is actually being reversed). If it is argued that the shear stress induces a phase change, then it should be the magnitude (and not the direction) of the stress that is important. Thus phase segregation should occur independent of whether the flow field is steady or periodic. The particular model proposed by Rangel-Nafaile et al.[33] makes use of Marrucci's earlier work[25] in which it is shown that for the dumbbell model (i.e., for very low concentration solutions where entanglement effects can be ignored) the stored energy is related to the trace of the stress tensor. Rangel-Nafaile et al. have calculated the trace of the stress tensor from the first normal stress differnce and used this to determine the stored elastic energy and hence to calculate any changes in phase stability. We note that this model (which appears to work even at rather high concentrations where it is unlikely that the constitutive equations used by Marrucci are valid) would suggest that phase separation will be unaffected if we change from a steady to a periodic flow field provided that the magnitude of the shear rate remains the same.

In the present work we have set out to use oscillatory flow fields, with a constant magnitude of shear rate, to test when adsorbtion–entanglement layers and liquid–liquid phase separation occur. Four distinct types of behavior have been found, depending on the shear rate. Once these four types of behavior had been identified several further experiments using sudden changes in shear rate were conducted to find out how the boundaries between them varied with polymer concentration and temperature. We shall argue that these behaviors correspond to the following: normal flow unhindered by any adsorption or phase separation, spontaneous liquid–liquid phase separation, the formation of topological adsorbtion–entanglement layers, and stress-induced, liquid–liquid phase separation nucleated at a preexisting adsorption–entanglement layer.

Experimental Details

Materials. The polymer was a poly(methyl methacrylate) (PMMA) with weight-average molecular weight ca. 7×10^6 and with a broad (but unknown) distribution of molecular weight. The solvent used was laboratory grade dimethyl phthalate (DMP). This is the same system used in previous studies of adsorption–entanglement layers.[24,26-28] Solutions were prepared by dilution from a 10% stock solution, which was itself prepared by first dissolving the polymer in chloroform and then adding DMP and evaporating the chloroform.

Apparatus. The rheological measurements were performed with a Rheometrics RMS800 mechanical spectrometer equipped with a 100 g cm force rebalance transducer. In all the experiments the cone and plate geometry was used, the cone had a diameter of 50 mm and an angle of 0.04 rad. In most experiments the plate was a metal cup with a flat bottom; the top of the cup was kept covered with a metal plate to avoid evaporation of the solvent (n.b., DMP has a low volatility and is an ideal solvent for this type of work). The temperature was varied by using a forced air oven surrounding the cup. In a few experiments, carried out at room temperature, a glass cup was

used to permit observations of turbidity changes.

Three types of experiment were carried out: (i) Steady dynamic: In this mode a triangular wave displacement was applied to the cup with a constant amplitude and very slowly increasing frequency. (ii) Steady—In this mode constant rate of rotation in one sense was applied to the cup. (iii) Step rate—In this mode the rate of rotation applied to the cup was held at one constant value and then abruptly changed to a lower constant value.

Assessment of the Static "Phase Diagram". In addition to the rheological experiments, the liquid–liquid phase separation of the PMMA–DMP system was examined under static conditions. The method used was to cool solutions with various concentrations and then observe the phase boundary by noting the temperature of the change from a turbid to a clear liquid or subsequent slow reheating. All the assessements of turbidity were made visually.

Results and Discussion

(1) Experiments To Determine Types of Rheological Behavior. The first group of experiments, designed to determine types of behavior by using an oscillating shear, were all carried out on a 2% wt/vol solution of PMMA in DMP. We have chosen to represent our data in all our figures and tables in terms of the actual measured quantities, torque and rotation rate, rather than the more usually quoted shear stress and strain rates (although these can readily be obtained from the geometrical data in the experimental section). We have done this, as we believe (and will show) that these solutions are liable to form thick layers at the surfaces of the cone and plate. Accordingly, we avoid errors that could easily be made in calculating shear stress and strain rates.

(A) Steady Dynamic Experiments. In these experiments a constant shear rate was applied to the sample and after some fixed amplitude the sense of rotation was reversed—so as to produce a triangular wave in shear and a square wave in shear rate. For a Newtonian liquid the response would thus be a square wave in torque. In practice, four distinctly different types of behavior were observed. For rotation speeds of less than ca. 2×10^{-5} rad/s the torque response was the simple square wave, for all amplitudes investigated (up to 3 rad). For rates of 2×10^{-5} to 10^{-2} rad/s the torque response was a simple square wave at small amplitudes (lessa than ~0.5–1 rad depending on the rate); at higher amplitudes the magnitude of the torque increased to a plateau value during the cycling. For rates of 10^{-2} to 2 rad/s the torque response at small amplitudes (less than ~0.5–0.3 rad depending on the rate) was again a simple square wave; at higher rates the magnitude of the torque continued to rise with no sign of a plateau being reached. At rates higher than ~3 rad/s the magnitude of the torque fluctuated between wide limits. All this behavior is illustrated by the diagram in Figure 1. Here traces representing typical torque/time behavior are superimposed on a diagram showing the amplitudes and rates at which each type of behavior was observed.

(B) Steady Experiments. In these experiments the same basic four types of behavior were observed. At low rates (~10^{-5} rad/s) the torque remains constant with time; at higher rates (up to ~10^{-2} rad/s) the torque, after a short time, starts to increase to a plateau value; at still higher rates (up to ~2 rad/s) the torque continues to increase throughout the experiment with no evidence for a plateau; while at the rates above 2 rad/s a widely oscillatory torque is observed. All this behavior is illustrated in Figure 2 by selected plots of torque against angle of rotation of the bottom plate (which is equivalent to time of rotation).

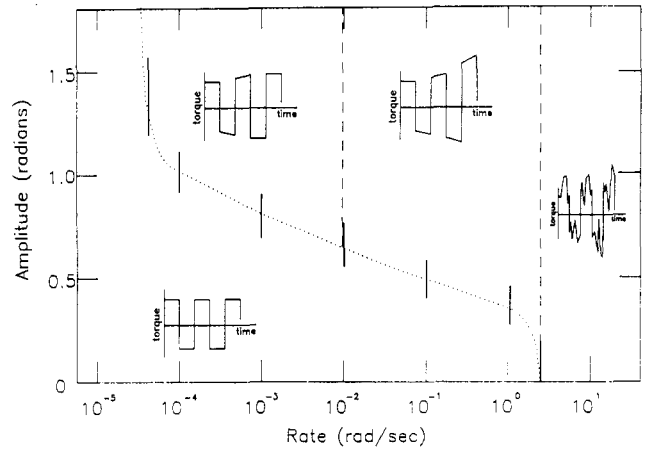

Figure 1. Diagram indicating the various types of behavior observed in oscillatory shear of a 2% wt/vol solution of PMMA in DMP. The horizontal axis is the applied rotation rate of the plate (n.b., a triangular displacement was applied to the plate so as to maintain a constant alternating shear rate). The vertical axis represents the amplitude of the oscillation (in radians). The sketches of torque against time show typical behavior at particular amplitudes and rates. The solid bars indicate the range of amplitudes over which the transition from "normal" to "abnormal" behavior occurs. The dotted line is drawn through these data. The vertical dashed lines indicate the rates at which the type of abnormal behavior changes: at ca. 10^{-2} rad/s from a rise in the magnitude and the torque to a plateau value, to a continuous rise in the magnitude of torque; at ca 2 rad/s to a violently fluctuating torque.

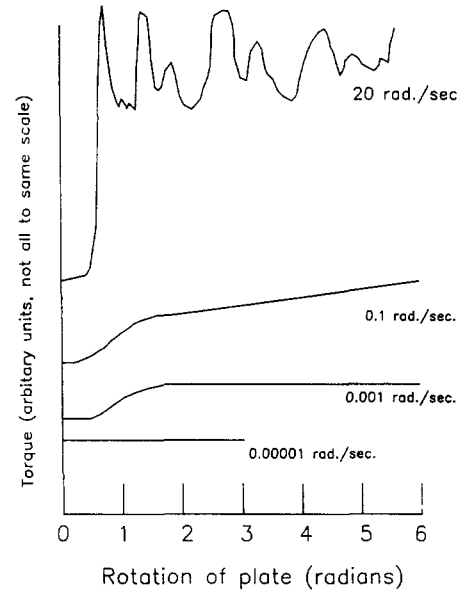

Figure 2. Series of plots showing typical results of experiments in continuous shear at a variety of rotation rates using the same solution as in Figure 1. The plots are in the form of torque against rotation angle of the bottom plate (this permits data covering a very wide range of rates to be presented on a common diagram). N.b., the torque scale is different for each rate.

(C) Visual Observations of Turbidity. In a few experiments, carried out at room temperature, a glass-bottom plate was used so that a visual assessment of solution clarity could be made. By use of this system a change in the clarity of the solution could be observed, as a degradation of the image of machining marks on the stationary cone, at high shear rates. No sudden change from a clear to a turbid solution occurred; instead the image of the marks on the cone gradually became less well defined as the rotation rate rose above ~2 rads/s.

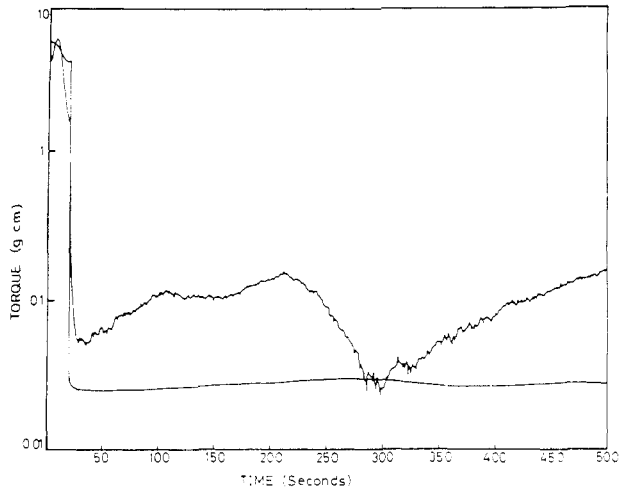

Figure 3. Recorded torque during experiments where the solution (as in Figure 1–4) was initially sheared for 20 s at 20 rad/s and then at a lower rate. The results for two different experiments using second rates of 1.5×10^{-2} and 9.9×10^{-3} are shown. Upper irregular cone is at 1.5×10^{-2} rad/s and lower smooth curve at 9.9×10^{-3} rad/s.

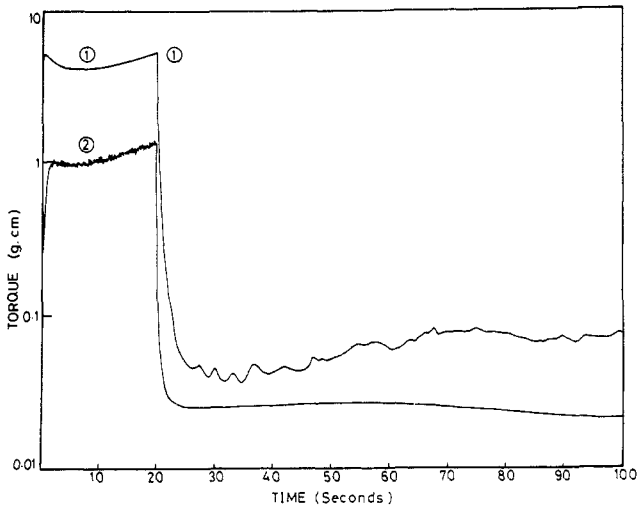

Figure 4. Recorded torque during two experiments where the solution was sheared at (1) initially 3 rad/s and (2) 0.8 rad/s for 20 s and subsequently at 2.5×10^{-2} rad/s.

(2) Interpretation of Results Using the 2% wt/vol Solution. The results described above clearly demonstrate the existence of four distinct types of behavior (in the presently used 2% wt/vol solution), depending on both strain rate and amplitude. These may be summarized as follows: (1) Very low rates, up to 2×10^{-5} rad/s—"normal" behavior. (2) Low rates, 2×10^{-5} to 10^{-2} rad/s—"normal" behavior in small-amplitude oscillating flow; shear stress increases to plateau value in continuous flow. (3) Intermediate rates, 10^{-2} to 2 r/s—"normal" behavior in small-amplitude oscillating flow; shear stress increases continuously in continuous flow. (4) High rates, greater than 2 rad/s—large, erratic, oscillations in shear stress; solutions start to become turbid.

The arguments made in the Introduction suggested that adsorption–entanglement layer formation should be suppressed in oscillating flows, while stress-induced liquid–liquid phase segregation should not. Accordingly, it can be deduced that the behavior in 2 (and possibly also 3) is due to the formation of adsorption–entanglement layers, while that in 4 is caused by flow-induced liquid–liquid phase segregation.

The difference between 2 and 3 suggests the interpretation that in 2 the surface layer stops growing at a finite

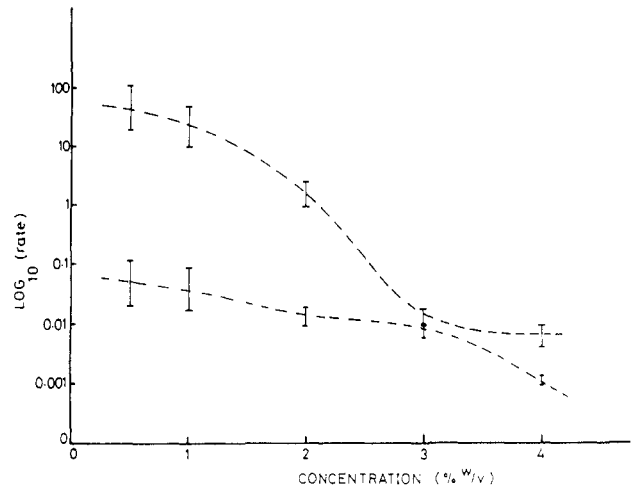

Figure 5. Graph showing the rates at which the changes between the various behaviors occur as a function of solution concentration at 18 °C. Upper cone relates to the 3 → 41 boundary and lower curve to its 2 → 3 boundary as described in the text.

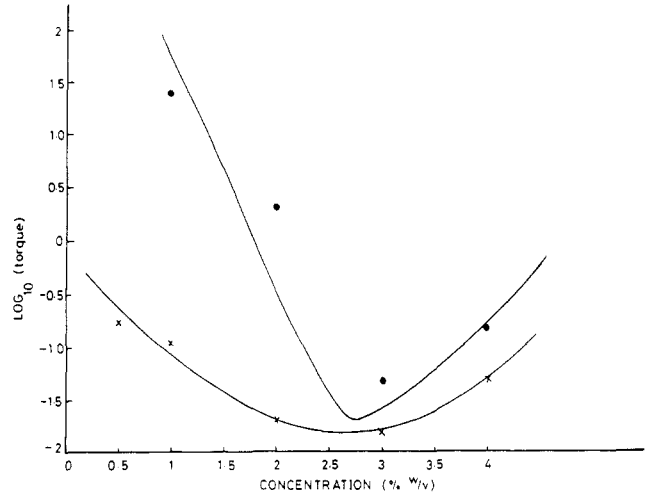

Figure 6. Graph showing the torques at which changes between the various types of behavior occur as a function of solution concentration at 18 °C. Upper curve relates to 3–4 boundary and lower curve to 2–3 boundary.

thickness, while in 3 it continues to grow well beyond that limit. The reasons for this will be discussed in more detail later. Now that these different types of behavior have been identified, we are in a position to map out the boundaries between the regions (especially 2 and 3 and 3 and 4) as a function of solution concentration and temperature and to investigate the possibility of any hysterisis effects in crossing the boundaries.

(3) Step Rate Experiments and the Phase Boundaries. A convenient way to find the boundaries between the various types of behavior is first to induce the behavior as in 4 above in shearing at a high rate and then reducing the rate in a sudden step and observing the corresponding torque response. Typical results of this kind of experiment are shown, for the 2% wt/vol solution, in Figure 3. The torque at the initial, high rate (20 rad/s) displays the fluctuations characteristic of type 4 behavior. However, when the rate is reduced either of two behaviors are seen at the lower rate. If the second rate is low enough then the torque rapidly decays and reaches a new, steady value; at higher second rates the torque level decreases but the torque continues to show large oscillations. The rate at which the transition in the above behavior occurs is very sharply defined; in this case it takes place between 9.8×10^{-3} and 1×10^{-2} rad/s.

Table I
Measured Torque Values for Boundaries (g cm)[a]

temp, °C	concentration, % wt/vol									
	0.5		1.0		2.0		3.0		4.0	
	nuc	spin	nuc	spin	nuc	spin	nuc	spin	nuc	spin
5	0.08		0.02		0.006	0.05	*b*	0.006	0.006	0.008
10	0.13		0.04		0.008	0.5	0.008	0.015	0.01	0.04
18	0.17		0.11		0.02	2	0.015	0.05	0.04	0.25
31	3.1		0.63		0.1	4.0	0.06	0.08	0.1	0.2
40			3.0		0.32		0.13	0.25	0.2	0.3
50					2.5		0.6		1.5	3.0

[a] In this table we have quoted some torque values less than 0.01 g cm—these arise from experiments in which the transducer gave a good steady signal; however, we believe that they should be treated with caution. In general, we expect the error in all the measurements to be ±0.01 g cm. [b] Too low to measure.

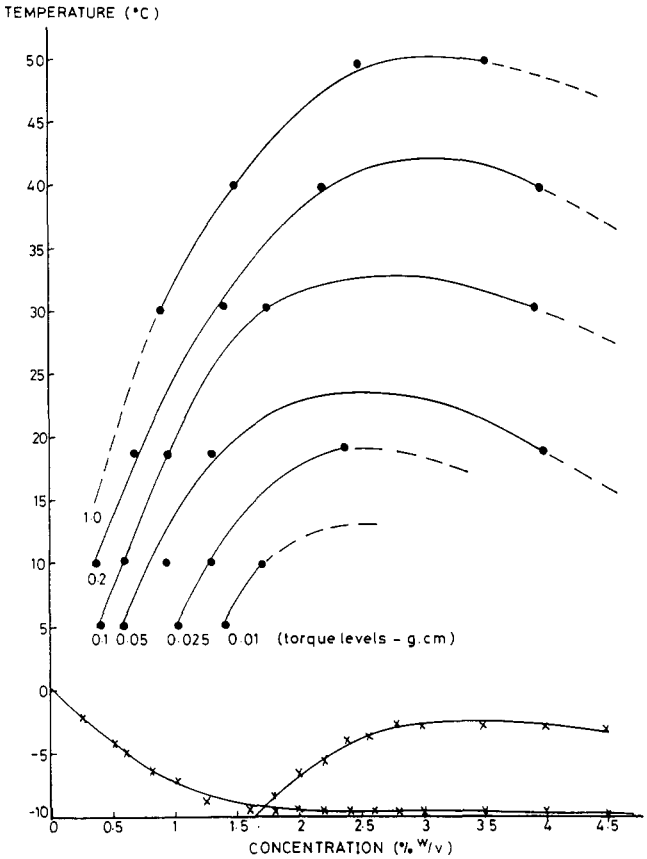

Figure 7. Schematic "phase diagram" for the PMMA/DMP system. The crosses and the lines drawn through them (lowest curves) represent the static phase diagram; at polymer concentrations up to ~1.6% wt/vol the solution freezes; at higher concentrations some liquid–liquid phase separation can be detected above the melting of the solid system. The solid circles in the rest of the diagram and the lines drawn through them represent the phase boundaries at constant torque levels (as extrapolated from graphs such as Figure 8).

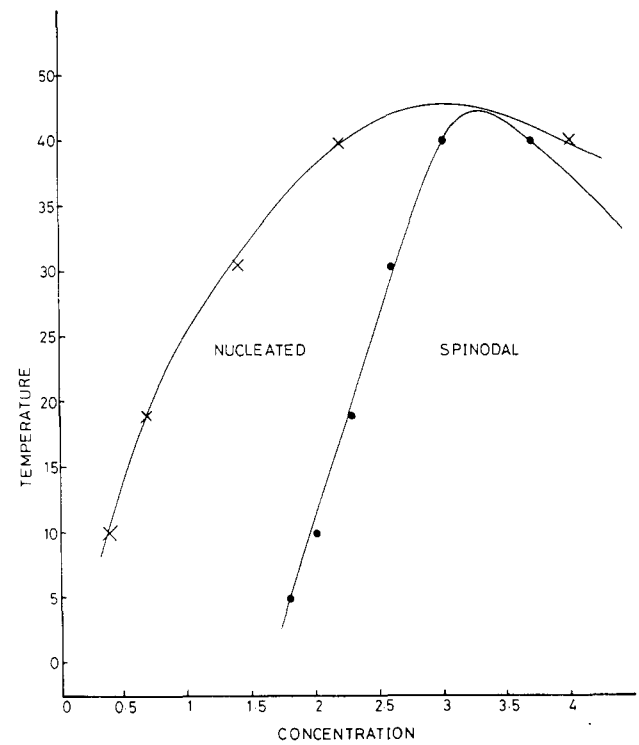

Figure 8. Proposed phase diagram, including the spinodal boundary at a torque level of 0.2 g cm.

It should be noted that the transition from type 3 behavior to type 4 on increasing the shear rate occurs at ca. 2 rad/s, while on decreasing the rate the transition from type 4 to type 2 behavior occurs at the lower rate of ca. 10^{-2} rad/s. Furthermore, this transition from type 4 behavior on reducing the rate corresponds closely with the previously observed transition between behaviors 2 and 3. If we interpret these results in terms of a phase diagram, with shear rate rather than temperature as the thermodynamic variable, then we can assign the transition between behavior 3 and 4 on increasng the rate to spontaneous liquid–liquid phase separation (i.e., to the spinodal curve). Similarly we can assign the transitiion from 4 to 2 on decreasing the rate (and from 2 to 3 on increasing the rate) to the "equilibrium" coexistence curve.

Region 3, by this argument, lies between the phase equilibrium boundary and the spinodal—thus in conventional terms it corresponds to a region where liquid–liquid phase segregation requires a nucleus to start it off. If there already is a layer of more concentrated polymer solution at the surface (an adsorption–entanglement layer), it could act as such a nucleus. Accordingly we argue that the behavior in region 3 corresponds to the formation of an adsorption–entanglement layer followed by the growth of this layer due to stress-induced liquid–liquid phase segregation.

The flow rate associated with the boundary between 3 and 4 can also be conveniently found by a step rate experiment. If the initial rate is varied and the final rate is kept fixed only slightly above the 2–3 boundary then, as is illustrated in Figure 4, two types of behavior are observed at the final rate. When the initial rate is less than the rate at the 3–4 boundary, the torque at the final rate remains more or less constant (curve 2 in Figure 4) (i.e., it behaves as if it had no prehistory). However, when the initial shearing induces phase segregation, the torque

Table II
Extrapolated Values of Concentrations at Boundaries

	torque levels											
	0.01		0.025		0.05		0.1		0.2		1.0	
temp, °C	nuc	spin	nuc	spin	nuc	spin	nuc	spin	nuc	spin	nuc	spin
5	1.4/-	2.4/-	1.0/-	2.1/-	0.6/-	2.0/-	0.4/-	1.9/-		1.8/-		1.6/-
10	1.7/4	2.5/3.5	1.3/-	2.3/3.8	0.8/-	2.2/-	0.6/-	2.1/-	0.4/-	2.0/-		1.7/-
18			2.3/3.6	2.75	1.3/4	2.6/3.5	0.9/-	2.4/3.8	0.7/-	2.3/-		2.3/-
31							2.0/3.9	2.9/3.5	1.4/-	2.6/-	0.9/-	2.3/-
40									2.2/4	3.0/3.7	1.5/-	2.5/-
50											2.5/3.5	2.7/3.3

Table III
Assignment of Previously Observed Flow Anomalies

polymer	solvent	flow geometry	type of behavior	ref
atactic polystyrene	toluene	capillary	*c*	1–4, 31
	decalin	capillary	*c*	1–4, 31
	chloroform	capillary	*c*	13–17
	Avoclor	cone & plate	*a* or *b*	5, 8
	dimethyl phthalate	cone & plate	*a*	10
	dioctyl phthalate	couette	*b* or *c*	23
	dioctyl phthalate	capillary	*b*	23
polyethylene	xylan	couette	*b*	20
	decalin	couette	*a*	36
	decalin	capillary	*b*	2–4
poly(ethylene oxide)	Avoclor	cone & plate	*a*	5, 9
polyacrylamide	water	capillary	*c*	18
proteins	water	oscillating plate	*a*	19
poly(vinyl alcohol)	water	couette	*a*	20
tobacco mosaic virus	water	couette	*b*	21
poly(methyl methacrylate)	dimethyl phthalate	cone & plate	*a* and *b*	10
	dimethyl phthalate	couette	*b*	1–3, 5
	dimethyl phthalate	capillary	*b*	1
	chloronaphthalene	cone & plate	*b*	5
	chloronaphthalene	couette	*b*	2
	xylene	couette	*b*	2
	Avoclor	cone & plate	*a*/*b*	1–4

[a] Spinodal phase separation. [b] Nucleated phase separation. [c] Adsorption–entanglement layers.

at the final rate is significantly higher and oscillates in an unstable fashion.

These simple step rate experiments can thus be used to map out the phase boundaries as a function of solution concentration and temperature. Figure 5 shows how the rates at the two boundaries (2–3 attributed to the equilibrium boundary and 3–4 attributed to the spinodal boundary) vary with solution concentration at 18 °C. An alternative way to present the same data is to plot the torques at which the boundaries occur—these are the *initial* torques at the various rates as measured in continuous shear (i.e., the torques at zero rotation angle in Figure 2). Such a plot is shown in Figure 6. As seen, the data points now begin to define lines more like those in a conventional phase diagram with torque replacing temperature as a thermodynamic variable. These experiments were repeated over a range of temperatures and the results are summarized in Table I.

(4) Construction of the Phase Diagram. Binary phase diagrams for polymer solutions are usually presented with only two axes, temperature and concentration; however, the results of the preceding section suggest that for flowing systems, a third axis, the shear stress (or torque), should also be used. A convenient way to represent this is to draw the temperature–concentration phase diagram at various torque levels. The concentrations at the fixed torque levels have simply been read off diagrams such as Figure 6. The resulting phase diagram is shown in Figure 7, together with the phase boundary found under static conditions as described earlier. The spinodal boundaries have been omitted for clarity; an example showing both the phase and spinodal boundaries for a particular torque level is shown in Figure 8, and the data used are presented in Table II.

(5) Adsorption–Entanglement Layers and Flow-Induced Liquid–Liquid Phase Separation. The simple picture that has emerged from the present study allows the reinterpretation of the results of many earlier studies. The types of behavior that may, in the present picture, be attributed to the formation of adsorption–entanglement layers can be summarized as follows. The layers will grow to a finite thickness significantly greater than the radius of gyration of the polymer molecules (typically this will be a few micrometers). The presence of the layers will be most easily recorded by their effect on the flow; in constant rate experiments (as in the present work) a small increase in recorded force (torque in the present case) to a plateau value will occur. In constant pressure experiments a reduction in flow rate to a constant value will be observed. Further, as in fact registered by capillary viscometry[29] and utilized in defining error sources in measurements of intrinsic viscosity,[31] the buildup of such layers may be expected to be more pronounced in good solvent systems where the polymer coils are expanded (so that there is a higher probability of interaction). Spontaneous liquid–liquid phase separation will be characterized by the occurence of unstable flows; such indeed are reflected by fluctuations in recorded stress, or flow rate, depending on the flow system. Such systems may also show the presence of "gellike" particles or turbidity. Finally, if liquid–liquid phase separation occurs by a nucleation and growth process, layers will form at surfaces and grow until a stable two-phase system has been established. The characteristic rheolog-

ical behavior will then be a continuous increase in stress or decrease in flow rate depending on the flow system. In some cases (especially in constant rate experiments) the layers formed at the surfaces may be torn away by the increasing stress across them as they grow; this would be manifested by the recorded stress rising to a peak value and then decreasing as is indeed frequently observed.[5,6]

For those interested we should note here that Magda and Larson[36] have shown in certain Boger fluids consisting of solutions of high molecular weight polyisobutylene that a flow instability of the type predicted by Phan-Thien[37,38] can lead to time-dependent viscous behavior, where the shear stress and normal stress both start to rise during continuous shearing at constant shear rate. Such behavior is characterized by its occurrence above a critical Wiessenberg number and not at a critical strain rate. The value of the critical Wiessenberg number may be calculated if the fluid is assumed to behave as an Oldroyd-B fluid.[38-41] For the system we have been using the critical Wiessenburg number would be ~10, whereas the transitions we have observed occur at Wiessenburg numbers of the order of unity, or less. Thus, we do not believe that these transitions can be attributed to a Phan-Thien flow instability.

There are many earlier works that have recorded anomalous flow behavior (see, e.g., ref 1–35); some of these have been invoked by ourselves previously as examples of adsorption–entanglement layer formation[26] and by others as flow-induced liquid–liquid phase segregation.[33] The criteria outlined above can be applied to these works and the behavior can (in most cases) thus be attributed to (a) spinodal phase separation, (b) nucleated phase separation, or (c) adsorption–entanglement behavior. We have attempted to do this on the basis of information available to us and the results are summarized in Table III.

One of these entries requires some further discussion. In the work from this laboratory by Hikmet et al.[26] with the identical PMMA/DMP system used in the present work, the Couette viscometry data show a series of peaks in the measured torque, while direct observation correlates these peaks with the growth of thick layers at the inner cylinder wall. In this case the rheological data suggest spinodal decomposition, while the observations of layer formation are indicative of nucleation. Comparison with the results in the present work suggests that these data were collected at rates close to but within the spinodal boundary. The appearance of a layer at the inner cylinder wall may, at first sight, seem to contradict this assertion. However, if phase separation occurs first in the bulk of the solution, then the concentrated phase, which in this case is less dense than the solvent, will by the centripetal forces move to the inner cylinder wall and give the appearance of a static layer. This would also explain why the layer appeared only at the inner (and not the outer) cylinder wall in the course of that work.

Conclusions

The work described here has shown the existence of four distinct types of rheological behavior in high molecular weight PMMA solutions, depending on the shear rate. These types of behavior have been identified as (i) normal behavior, (ii) growth of adsorption–entanglement layers, (iii) flow-induced nucleated liquid–liquid phase segregation, and (iv) spinodal decomposition induced by flow.

A phase diagram for the system PMMA/DMP in which the applied shear stress is treated as a thermodynamic variable has been proposed.

Acknowledgment. We thank the BP Venture Research Unit for supporting this work.

Registry No. PMMA, 9011-14-7; DMP, 131-11-3.

References and Notes

(1) Peterlin, A.; Turner, D. T. *Polym. Lett.* **1965**, *3*, 517.
(2) Peterlin, A.; Quan, C.; Turner, D. T. *Polym. Lett.* **1965**, *3*, 521.
(3) Peterlin, A.; Turner, D. T.; Philippoff, W.; *Kolloid Z.* **1965**, *204*, 21.
(4) Burrow, S.; Peterlin, A.; Turner, D. T. *Polym. Lett.* **1964**, *2*, 67.
(5) Matsuo, T.; Pavan, A.; Peterlin, A.; Turner, D. T. *J. Colloid Interface Sci.* **1967**, *24*, 241.
(6) Narh, K. A.; Barham, P. J.; Keller, A. *Macromolecules* **1982**, *15*, 464.
(7) Pennings, A. J. *J. Polym. Sci., Polym. Symp.* **1977**, *59*, 55.
(8) Monk, P.; Peterlin, A. *Trans. Soc. Rheol.* **1970**, *14*, 65.
(9) Laufer, Z.; Jalink, M. L.; Staverman, A. J. *J. Polym. Sci., Polym. Chem. Ed.* **1973**, *11*, 3005.
(10) Lodge, A. S. *Polymer* **1961**, *2*, 195.
(11) Adams, N.; Lodge, A. S. *Philos. Trans. R. Soc.* **1964**, *A256*, 149.
(12) Zwijnenburg, A. Ph.D. Thesis, Groningen, 1978.
(13) Öhrn, O. E. *J. Polym. Sci.* **1956**, *19*, 199.
(14) Öhrn, O. E. *J. Polym. Sci.* **1955**, *17*, 132.
(15) Streeter, D. J.; Boyer, R. F. *J. Polym. Sci.* **1954**, *14*, 5.
(16) Umstätter, H. *Makromol. Chem.* **1954**, *12*, 94.
(17) Batzer, H. *Makromol. Chem.* **1954**, *12*, 145.
(18) Cohen, Y.; Metzner, A. B. *Macromolecules* **1982**, *15*, 1425.
(19) Ohnishi, T. *J. Polym. Sci.* **1962**, *62*, 542.
(20) Peter, S.; Noetzel, W. *Kolloid Z.* **1962**, *183*, 97.
(21) Joly, M. *Kolloid Z.* **1962**, *182*, 133.
(22) Steg, I.; Katz, D. *J. Appl. Polym. Sci.* **1965**, *9*, 3177.
(23) van Strate, G.; Philippoff, W. *J. Polym. Sci., Polym. Lett. Ed.* **1974**, *12*, 267.
(24) Hikmet, R. A. M. Ph.D. Thesis, Bristol, 1986.
(25) Marrucci, G. *Trans. Rheol. Soc.* **1972**, *16*, 321.
(26) Hikmet, R. A. M.; Narh, K. A.; Barham, P. J.; Keller, A. *Progr. Colloid Polym. Sci.* **1985**, *71*, 32.
(27) Narh, K. A.; Barham, P. J.; Hikmet, R. A. M.; Keller, A. *Colloid Polym. Sci.* **1986**, *264*, 507.
(28) Barham, P. J.; Hikmet, R. A. M.; Narh, K. A.; Keller, A. *Colloid Polym. Sci.* **1986**, *264*, 515.
(29) Barham, P. J. *Colloid Polym. Sci.* **1986**, *264*, 507.
(30) Barham, P. J. *Colloid Polym. Sci.* **1987**, *265*, 584.
(31) Barham, P. J.; Keller, A. *Colloid Polym. Sci.* **1989**, *267*, 494.
(32) Hand, J. M.; Williams, M. C. *Chem. Eng. Sci.* **1973**, *28*, 63.
(33) Rangel-Nafaile, C.; Metzner, A. B.; Wissbrun, K. F. *Macromolecules* **1984**, *17*, 1187.
(34) Wolf, B. A. *Macromolecules* **1984**, *17*, 615.
(35) Kramer, H.; Wolf, B. A. *Makromol. Chem., Rapid Commun.* **1985**, *6*, 21.
(36) Magda, J. J.; Larson, R. G. *J. Non Newtonian Fluid Mech.* **1988**, *30*, 1.
(37) Phan-Thien, N. *J. Non Newtonian Fluid Mech.* **1983**, *13*, 325.
(38) Phan-Thien, N. *J. Non Newtonian Fluid Mech.* **1985**, *17*, 37.
(39) Prilutski, G.; Gupta, R. K.; Sridhar, T.; Ryan, M. E. *J. Non Newtonian Fluid Mech.* **1983**, *12*, 233.
(40) Jackson, K. P.; Walters, K.; Williams, R. W. *J. Non Newtonian Fluid Mech.* **1984**, *14*, 173.
(41) Binnington, R. J.; Boger, D. V. *J. Rheol.* **1985**, *29*, 887.